

Investigation of High-Performance ITO-Stabilized ZnO TFTs With Hybrid-Phase Microstructural Channels

Sunbin Deng, Rongsheng Chen, *Member, IEEE*, Guijun Li, Zhihe Xia, Meng Zhang, *Member, IEEE*, Wei Zhou, Man Wong, *Senior Member, IEEE*, and Hoi-Sing Kwok, *Fellow, IEEE*

Abstract—In this paper, the properties of hybrid-phase microstructural indium tin oxide-stabilized ZnO thin films and the relevant high-performance thin-film transistors (TFTs) were systematically investigated. The optically extracted Urbach energy revealed that such thin films owned less band-tail state trapping in comparison with that of the corresponding amorphous thin films. This was determined by better atomic arrangement and might realize higher drift mobility theoretically. The influence of deposition parameters such as oxygen partial pressure ratio (P_{O_2}) and direct-current power (P_{DC}) on thin films was discussed in detail. Then, the TFTs with optimal co-sputtering conditions were fabricated. Such devices exhibited a typical field-effect mobility of $26.1 \text{ cm}^2/\text{V}\cdot\text{s}$, threshold voltage of 0.5 V , on-off ratio of over 10^9 , and extremely low subthreshold swing of 89 mV/decade . Meanwhile, the spatial uniformity, air stability, and repeated switching behavior of devices were demonstrated to be excellent.

Index Terms—Hybrid-phase microstructure, ITO-stabilized ZnO, thin-film transistor (TFT).

I. INTRODUCTION

OWING to merits such as low manufacturing costs and temperature, excellent optical transparency, and reasonable electrical properties, many recent flat-panel display (FPD) products adopt metal-oxide (MO) thin-film transistors (TFTs) in their backplanes. Therein, amorphous indium gallium zinc oxide (a-IGZO) is one of the most prevalent channel choices [1]–[5]. Compared with the conventional hydrogenated amorphous silicon (a-Si:H), the superiorities of a-IGZO mainly

lie in its relatively high mobility ($5\text{--}10 \text{ cm}^2/\text{V}\cdot\text{s}$) and extremely low OFF-state current. These properties are necessary in high-definition and low-power-consumption applications, especially for small- or medium-size mobile devices. Although the mobility provided by the low-temperature polycrystalline silicon (LTPS) technology is higher, the electrical nonuniformity as a result of grain boundaries always hinders its infiltration in large-area display market [10], [11]. Contrastively, a-IGZO TFTs are compatible with FPD products with a wide range of backplane size, even though the production line expands beyond Gen 8.

However, when FPD technology develops toward super high resolution and frequency (e.g., over 7680×4320 resolution and $>120 \text{ Hz}$ frame rate) and narrow bezels involving system on panel technologies, the common a-IGZO TFTs seem difficult to offer enough driving capability [5]. Thus, many efforts by adjusting material composition or microstructure have been paid to boost the mobility of MO semiconductors beyond the general a-IGZO. In terms of material composition, the In/Ga/Zn atomic ratio in a-IGZO system was well studied and optimized [1], [12], [13]. In particular, the field-effect mobility could reach as high as $63.6 \text{ cm}^2/\text{V}\cdot\text{s}$ when a-IGZO channels (In:Ga:Zn = 71.2:21.3:7.5) were employed together with ALD SiO_2 gate dielectric layers [15]. Meanwhile, a plenty of a-IGZO counterparts with higher mobility such as IZO, ITZO, and ATIZO were also proposed [9], [16]–[18]. On the other hand, from the perspective of material microstructure, Yamazaki *et al.* reported a cloud-aligned composite IGZO with a common composition of In:Ga:Zn = 1:1:1, and a field-effect mobility of near $40 \text{ cm}^2/\text{V}\cdot\text{s}$ was obtained in TFTs [19]. Besides, Stewart and Wager [22] and Stewart *et al.* [23] also predicted an upper carrier mobility limit for amorphous semiconductors, because the carrier trapping in each material would significantly affect its actual drift mobility, which was closely associated with the nature of disorder. However, more highly ordered microstructure is not absolutely welcomed, especially considering the nonuniformity issue among LTPS TFTs. Therefore, both material composition and microstructure ought to be well taken into consideration. Combining with these two aspects, we previously proposed a kind of indium tin oxide (ITO)-stabilized ZnO thin films with hybrid-phase microstructure, and employed them as active layers in the bottom-contact top-gated TFTs [27].

Manuscript received February 28, 2017; revised April 15, 2017 and May 17, 2017; accepted May 30, 2017. This work was supported by the Research Grants Council, Hong Kong Government through the Theme-Based Research Project under Grant T23-713/11-1. The review of this paper was arranged by Editor K. C. Choi. (*Corresponding author: Rongsheng Chen.*)

S. Deng, G. Li, Z. Xia, M. Zhang, W. Zhou, M. Wong, and H.-S. Kwok are with the State Key Laboratory on Advanced Displays and Optoelectronics Technologies, Department of Electronic and Computer Engineering, The Hong Kong University of Science and Technology, Hong Kong (e-mail: sdengaa@connect.ust.hk).

R. Chen is with the School of Electronic and Information Engineering, South China University of Technology, Guangzhou 510640, China, and also with the State Key Laboratory on Advanced Displays and Optoelectronics Technologies, Department of Electronic and Computer Engineering, The Hong Kong University of Science and Technology, Hong Kong (e-mail: chenrs@scut.edu.cn).

Color versions of one or more of the figures in this paper are available online at <http://ieeexplore.ieee.org>.

Digital Object Identifier 10.1109/TED.2017.2711199

In this paper, the hybrid-phase microstructural ITO-stabilized ZnO thin films and the relevant TFTs were systematically investigated. Initially, the microstructural properties of thin films were characterized physically, and less band-tail state trapping was measured quantitatively. Then, the influence of deposition parameters such as oxygen partial pressure ratio (P_{O_2}) and direct-current power (P_{DC}) on thin films were discussed in detail. Afterward, it was found that the optimal top-contact bottom-gated TFTs could be obtained when P_{O_2} and P_{DC} were set as 40% and 120 W, respectively. The corresponding devices were operated with relatively high and spatially uniform electrical characteristics. Finally, the ambient instability of devices was well suppressed due to the *in situ* passivation of channels, and the switching behavior after repeated cycling was demonstrated to be good.

II. EXPERIMENT

The ITO-stabilized ZnO thin films with hybrid-phase microstructure were deposited on SiO₂/Si substrates at room temperature through magnetron co-sputtering 2-in circular ITO (90 wt% In₂O₃ and 10 wt% SnO₂) and ZnO targets. The ITO target was connected with a direct-current power source, whereas the ZnO target was sputtered using a RF one. The distance between substrates and targets was both 10 cm. The base pressure and working pressure in chamber were pumped to 5×10^{-6} and 3×10^{-3} Torr, respectively. During deposition, the total gas flow rate was 20 sccm, and the RF power (P_{RF}) was fixed at 150 W. The deposition time for all thin films was 20 min. To investigate the influence of P_{O_2} on thin films, P_{DC} was set to 120 W, and the flow rate of O₂ was tuned from 2 to 12 sccm; then, P_{O_2} accordingly varied from 10% to 60%. To study the influence of P_{DC} on thin films, P_{O_2} was kept at 40%, and P_{DC} was configured from 60 to 90, 120, and 150 W. For the crystalline phase characterization of thin films, an X-ray diffractometer (XRD, PANalytical Empyrean) with Cu K α radiation was used. It was operated in thin-film mode, and the angle between the X-ray and thin film surface was set to 0.5°. Then, the microstructure of thin films was further probed using a high-resolution field emission transmission electron microscope (HRTEM, JEOL JEM-2010HR). Additionally, an atomic force microscopy (AFM, Park XE150S) was used to analyze the surface morphology of thin films. The substrates were Si wafers coated by thermally grown SiO₂, which owned a surface root-mean-square (rms) roughness of ~ 0.1 nm. Besides, a UV-Visible spectroscopy (Perkin Elmer Lambda 20) was employed to obtain the absorption spectrum of thin films. To analyze the material composition and chemical states of oxygen, X-ray photoelectron spectroscopy (XPS) measurement was conducted on the Physical Electronics 5600 multitechnique system. For precise detection, the surface 5-nm-thick thin films were etched using Ar ions before XPS characterization. The thin-film resistivity was measured using a four-point-probe system (Lucas Pro4-640R). All of the thin films were thermally annealed at 300 °C in air before any characterizations mentioned above.

The schematic of the basic top-contact bottom-gated TFTs is shown in Fig. 1. The gate insulator herein employed the



Fig. 1. Schematic of the top-contact bottom-gated TFTs in this work.

thermally grown SiO₂ with less defects. This avoided the negative impact coming from the gate insulator layer as much as possible, and the influence of different active layers on the device electrical performance could be exclusively investigated. The whole fabrication processes started on 4-in heavily doped n-type Si wafers, which were coated by 120-nm-thick thermally grown SiO₂. After backside oxide removal in a buffered oxide etchant solution, the exposed Si would serve as the gate electrode. Then, 50-nm-thick active layers were deposited on substrates through magnetron co-sputtering ITO and ZnO targets at room temperature. The detailed deposition conditions were described above. Next, the active layers were patterned using the conventional photolithography and etched in diluted hydrofluoric acid. The width and length of channels were defined as 90 and 45 μ m, respectively. After photoresist stripping, a lift-off method was performed to form 150-nm-thick sputtered aluminum source and drain electrodes. Finally, the devices were subjected to thermal annealing at 300 °C in air. The electrical characteristics of TFTs were measured in the probe station using a semiconductor parameter analyzer (Agilent 4156C).

III. RESULTS AND DISCUSSION

A. Thin-Film Properties

Fig. 2(a) shows an XRD spectrum of the hybrid-phase microstructural ITO-stabilized ZnO thin films that deposited on SiO₂/Si substrates at room temperature. A relatively wide peak centered at around 33.5° can be detected. For reference, the XRD spectrum for substrates is also plotted, and no peak is observed. It means that there exist grains with a size of ~ 2 nm in the hybrid-phase microstructural thin films according to Scherrer's equation [27]. Since such peak corresponds to neither the diffraction peaks of polycrystalline ZnO films nor those of polycrystalline ITO films, the nanocrystals are composed of some complex compounds, rather than the segregated ZnO or ITO. Then, the hybrid-phase microstructure is further investigated using HRTEM, and the cross-sectional HRTEM image of thin films is shown in Fig. 2(b). For better recognition, pairs of arrows are employed to highlight several nanocrystals. The measured grain size is consistent with the XRD-derived result, and the interplanar crystal spacing is 0.28 ± 0.01 nm. Based on the information about XRD diffraction peak position and interplanar crystal spacing value, it can be inferred but not confirmed that the above nanocrystals are likely to consist of the homologous Zn_kIn₂O_(k+3) (where $k = 3, 4$), ilmenite ZnSnO₃, and spinel Zn₂SnO₄ compounds [28]. Different from conventional amorphous and polycrystalline phase, the columnar grains herein are sparsely interspersed in an amorphous matrix. Thus, we name it as the

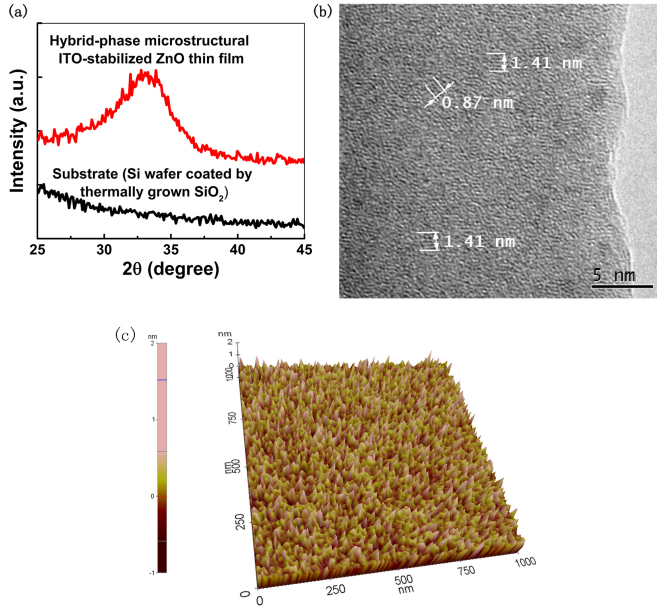


Fig. 2. (a) XRD spectra of the ITO-stabilized ZnO thin films with hybrid-phase microstructure and SiO₂/Si substrates. (b) Cross-sectional HRTEM image of the hybrid-phase microstructural thin films, and pairs of arrows are eye guides for recognition of nanocrystals. (c) AFM image of the surface of hybrid-phase microstructural ITO-stabilized ZnO thin film deposited on SiO₂/Si substrates.

“hybrid-phase” microstructure, and the “phase” herein refers to the microstructural phase of materials only, rather than the chemical phase of nanocrystals or amorphous matrix. Moreover, compared with the absolutely nanocrystalline thin films, the grain boundary density in the hybrid-phase microstructural thin films is expected to be lower. Considering the grain size is much smaller than the general transistor size, the device uniformity will not be affected. To better understand the microstructure, an AFM image describing the surface morphology of thin films is presented in Fig. 2(c). There are no apparent grains and grain boundaries observed. Meanwhile, the measured rms roughness within a $1 \times 1 \mu\text{m}^2$ region can be as low as 0.299 nm, which is potential to reduce the interfacial scattering and enhance the mobility of TFTs.

To identify the atomic disorder degree of the hybrid-phase microstructural ITO-stabilized ZnO thin films, the Urbach energy (E_U) is optically extracted from the absorption spectrum of materials. The extraction is referred to the empirical Urbach relation

$$\alpha = \alpha_0 \exp\left(\frac{h\nu - E_I}{E_U}\right) \quad (1)$$

where α_0 and E_I are the constants and $h\nu$ represents the incident photon energy. Fig. 3 describes the variation of $\ln(\alpha)$ as a function of $h\nu$ near the fundamental absorption edge of thin films, where E_U is equal to the reciprocal of the fitted straight line’s slope. For the hybrid-phase microstructural ITO-stabilized ZnO thin films, the extracted E_U is 111.9 meV, which is well situated between the value of polycrystalline ZnO (~ 67 meV) and the value of amorphous ITZO ($170 \sim 200$ meV) [29], [30]. It is suggested that the

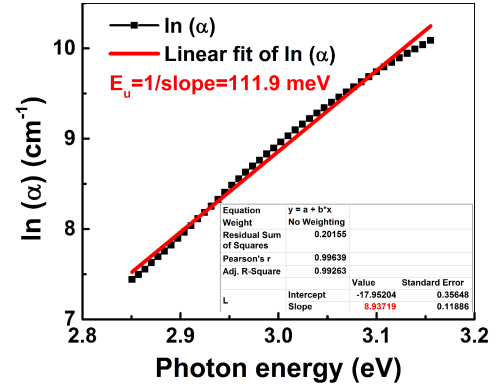


Fig. 3. Plot of $\ln(\alpha)$ versus incident photon energy near the fundamental absorption edge of hybrid-phase microstructural ITO-stabilized ZnO thin films. The Urbach energy is extracted from the reciprocal of the fitted straight line’s slope.

atoms in hybrid-phase microstructural thin films are better organized compared with those in amorphous thin films. This indicates less band-tail state trapping as well. To see the benefits, consider the equation described in the following:

$$\mu_{\text{drift}} = \frac{1}{1 + \frac{N_T}{N}} \quad (2)$$

where N , N_T , μ_{drift} , and μ_0 are the free carrier concentration, trapped carrier concentration, drift mobility, and trap-free mobility, respectively [23]. When the reduction of band-tail state trapping contributes to lower N_T , it is potential to realize less deviation from μ_0 and obtain higher theoretical from μ_{drift} . But this phenomenon herein is not as pronounced as that in the case of Si-based materials, because the large s orbitals of heavy metal cations are intrinsically helpful to realize less electron traps and relieve mobility degradation as a result of atomic disorder [4], [23], [31].

B. Influence of Oxygen Partial Pressure Ratio (P_{O_2})

Apart from band-tail state trapping, the internal oxygen vacancies (V_O) are the other particular part that affects the trap tendency in most n-type MO semiconductors [32]. Additionally, V_O is also closely linked with carrier capture/release and then with the electrical conductivity of MO thin films. It is believed that the concentration of V_O can be effectively controlled by modulating P_{O_2} ($P_{O_2} = O_2/(Ar + O_2)$) during deposition process [33]. To illustrate the relationship between P_{O_2} and V_O in the hybrid-phase microstructural ITO-stabilized ZnO thin films more clearly, XPS characterization was employed to analyze the chemical states of oxygen in the deposited thin films. As shown in Fig. 4(a)-(d), the XPS spectra of O 1s peak can be divided into three peaks O_I, O_{II}, and O_{III}, and further fitted by the Gaussian–Lorentzian deconvolution. Theoretically, O_I, O_{II}, and O_{III} peaks are relevant to the oxygen bonded in lattices (such as In-O, Sn-O, and Zn-O), oxygen deficiencies in lattices (such as V_O), and chemisorbed oxygen (such as the bonded oxygen in hydroxyl groups) or excess oxygen (such as interstitial oxygen), respectively [34]–[36]. These peaks are accordingly centered in 530.2 ± 0.1 , 531.5 ± 0.2 , and 532.2 ± 0.1 eV.

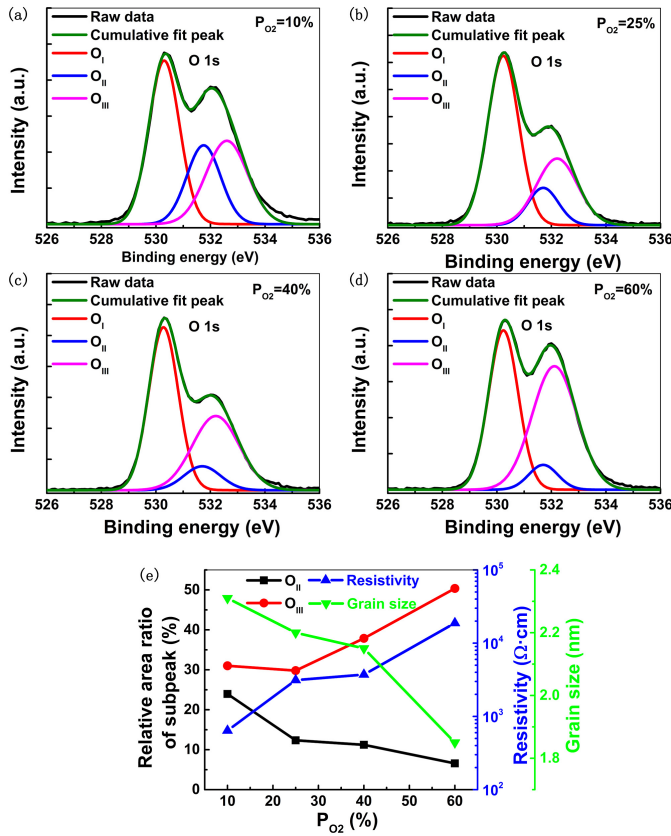


Fig. 4. XPS O 1s spectra of hybrid-phase microstructural ITO-stabilized ZnO thin films deposited under a P_{O_2} of (a) 10%, (b) 25%, (c) 40%, and (d) 60%. (e) Plot of the relatively area ratio of O_{II} and O_{III} peaks, thin film resistivity, and grain size variation as a function of P_{O_2} .

Fig. 4(e) exhibits that the relatively area ratio of O_{II} peak gradually reduces, whereas that of O_{III} peak keeps rising monotonically with the increase of P_{O_2} . It means that there is a negative correlation between P_{O_2} and V_O concentration when P_{O_2} varies from 10% to 60%. Meanwhile, the thin-film resistivity is found to climb by nearly two orders of magnitude. This is because V_O acts as a donor defect and contributes to electron conduction; then, higher P_{O_2} can compensate more portion of V_O and regulate the free carrier concentration of thin films toward a lower level [33], [37]. It is beneficial to suppress V_O -related traps and build enhancement-mode TFTs with low OFF-state current. Fig. 4(e) also exhibits that the average XRD-derived grain size shrinks by about 20% (from 2.31 to 1.85 nm) when P_{O_2} rises from 10% to 60%. For this phenomenon, some plausible explanations are provided as follows: 1) when P_{O_2} keeps increasing, it will introduce more and more oxygen ions during the sputtering process and cause severe bombardment on the growing thin films; then, the formed nanocrystals may be deteriorated, or the process of grain growth is probably restrained [38]–[40] and 2) the primarily sputtered nuclei in multicomponent ITO-stabilized ZnO material system are complex, which contains different species with diverse orientations; though the sufficient oxygen is helpful for individual nucleus expansion, it also aggravates the mutual growth competition among them at the same time, and then the shrinkage of grain size can be observed instead.

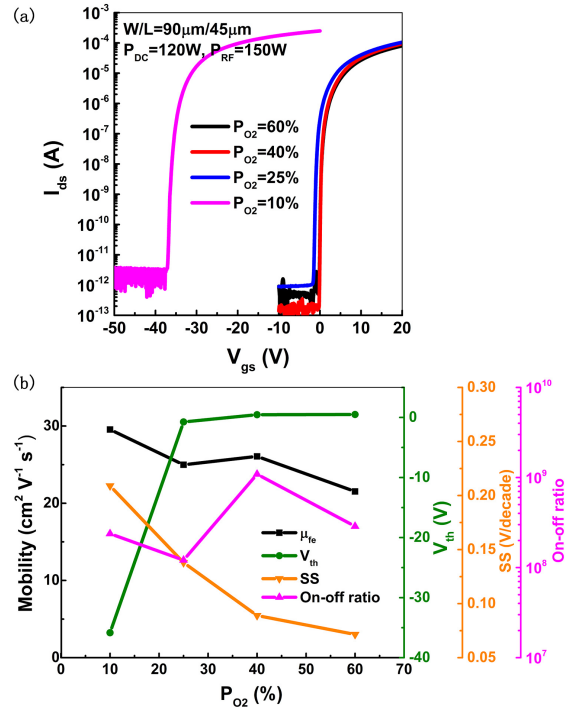


Fig. 5. (a) Transfer curves and (b) key electrical parameter variation of ITO-stabilized ZnO TFTs with hybrid-phase microstructural channels under different P_{O_2} .

Thus, high P_{O_2} will degrade atomic arrangement in the hybrid-phase microstructural thin films, resulting in more band-tail states. Therefore, P_{O_2} should be carefully adjusted in order to well balance the V_O -related trapping and also band-tail-state-related trapping.

The electrical performance variation of hybrid-phase microstructural ITO-stabilized ZnO TFTs under different P_{O_2} is also examined, as shown in Fig. 5. It can be observed that the electrical characteristics are significantly improved when P_{O_2} grows from 10% to 25%. Notably, threshold voltage (V_{th}) remarkably shifts from -35.85 to -0.75 V. This reflects that the free carrier concentration in active layers drops dramatically, which is consistent with the large decrease of relative area ratio of O_{II} peak [37]. With the further rise of P_{O_2} , the relative area ratio of O_{II} peak descends slowly, indicating that the concentration of V_O and the relevant free carrier concentration stays at quite a low magnitude. Thus, the positive shift of V_{th} becomes reasonably slight, even though P_{O_2} climbs to 60% eventually. The field-effect mobility (μ_{fe}) in this work is derived from the linear region of transfer characteristics and expressed as follows:

$$\mu_{fe} = \frac{Lg_m}{WC_{ox}V_{ds}} \quad (3)$$

where L , W , g_m , C_{ox} , and V_{ds} denote the channel length, channel width, transconductance, gate capacitance per unit area, and drain voltage (0.1 V), respectively. It is found that μ_{fe} reaches the maximum at $P_{O_2} = 10\%$, because the free carrier concentration in thin films should be enormous, referring to the extremely negative V_{th} . With the further rise of P_{O_2} , μ_{fe} drops but still stays high. This is probably owing to the well-defined

TABLE I
SOME MATERIAL MICROSTRUCTURE AND COMPOSITION RELATED PARAMETERS OF THIN FILMS UNDER DIFFERENT P_{DC}

P_{DC} (W)	Grain size (nm)	In/(In+Sn+Zn) (%)	Sn/(In+Sn+Zn) (%)	Zn/(In+Sn+Zn) (%)	(In+Sn)/(In+Sn+Zn) (%)	ITO deposition rate (nm/min)	ZnO deposition rate (nm/min)
60	1.97	18.9	1.3	79.8	20.2	2.0	
90	2.15	33.4	2.3	64.3	35.7	3.6	
120	2.26	38.6	2.7	58.7	41.3	4.4	3
150	2.38	46.7	3.3	50.0	50.0	5.1	

TABLE II
COMPARISON WITH SOME ITZO, ZnO, AND ITO TFTS PUBLISHED IN RECENT YEARS

Channel layer composition	Channel layer microstructure	Gate dielectric layer	μ_{fe} (cm ² /Vs)	V_{th} (V)	SS (decade/V)	On-off ratio	Reference
ITO-stabilized ZnO	hybrid-phase	SiO ₂	26.1	0.5	0.089	>10 ⁹	This work
ITZO	amorphous	Yb ₂ TiO ₅	27.9	0.52	0.203	1.1×10 ⁸	[6]
ITZO	amorphous	SiO ₂	27.59	-0.93	0.153	~10 ⁹	[7]
ITZO	amorphous	Al ₂ O ₃ /SiO _x /SiO ₂	31.08	0.28	0.096	~10 ⁷	[8]
ITZO	amorphous	SiO ₂	52.4±15.0	0.1±0.13	0.14±0.03	>2×10 ⁸	[9]
ITZO	amorphous	SiO ₂	21.67	2.46	0.568	—	[14]
ZnO	polycrystalline	HfO ₂	1.4	0.9	0.089	7.1×10 ⁸	[20]
ZnO	polycrystalline	Al ₂ O ₃	21.9	4.1	0.244	4×10 ⁸	[21]
ZnO	polycrystalline	Al ₂ O ₃	12	-1.2	0.3	~10 ⁸	[24]
ITO	amorphous	Ta ₂ O ₅	29.0±1.2	1.05±0.28	0.2	>10 ⁸	[25]
ITO	amorphous	Al ₂ O ₃	56.1	0.7	0.14	~10 ⁹	[26]

conduction band from 5s orbitals of indium and tin cations in thin film, which provides the intrinsically lower N_T and higher μ_0 in (2) [41]. Besides, the value of subthreshold swing (SS) always drops along with the increase of P_{O_2} . It indicates that the defects in devices are gradually passivated, which may also be responsible for the relatively high level of μ_{fe} .

C. Influence of Direct-Current Sputtering Power (P_{DC})

Table I lists the several typical parameters of channel layers under different P_{DC} for ITO sputtering, which are related to material microstructure and composition. Herein, P_{DC} varies from 60 to 150 W, while P_{RF} is fixed at 150 W. The grain size and (In + Sn)/(In + Sn + Zn) ratio are found to keep increasing with the rise of P_{DC} . However, the variation of (In + Sn)/(In + Sn + Zn) ratio is much more drastic than that of grain size. It is believed that P_{DC} has more influence on material composition, especially the content of indium and tin cations, rather than material microstructure. In general, the electron conduction band of a-IGZO is principally composed of the delocalized s orbitals of heavy metal cations [31]. Similarly, both indium and tin cations with 5s orbitals can also contribute to electron conduction in ITO-stabilized ZnO thin films. Therefore, P_{DC} should be one of the effective deposition parameters to adjust device electrical characteristics. Fig. 6(a) and (b) shows the transfer curves and the key electrical parameter variation of ITO-stabilized ZnO TFTs under different P_{DC} , respectively. It is found that the key electrical parameters of devices are all

improved distinctly when P_{DC} is boosted from 60 to 90 W. Within the same interval, the ITO deposition rate (from 2 to 3.6 nm/min) surpasses the ZnO deposition rate (3 nm/min). Such consistency also indicates that the content of ITO in active layers affects the electrical performance of devices significantly [18], [42]. When P_{DC} further climbs from 90 to 150 W, the devices behave with minor variation, even though (In + Sn)/(In + Sn + Zn) ratio still grows. However, it does not mean over high P_{DC} is acceptable. For example, indium cations can substitute zinc cation sites and release electrons, and then V_{th} will be negatively shifted [43], [44]. This phenomenon is indeed observed in Fig. 6(b) when P_{DC} climbs from 90 to 150 W. Therefore, P_{DC} needs to be well modulated together with the other deposition parameters such as P_{O_2} and P_{RF} . According to the overall electrical characteristics of devices, the optimal P_{DC} herein should be set as 120 W.

D. Performance of Optimal Devices

Referring to the discussion above, the optimal hybrid-phase microstructural ITO-stabilized ZnO TFTs with the basic top-contact bottom-gated architecture can be fabricated when P_{O_2} is 40% and P_{DC} is 120 W. Under these conditions, the XPS results show that the percentage of indium, tin, and zinc occupied among metal cations are 38.6%, 2.7%, and 58.7%, respectively; meanwhile, the average XRD-derived nanocrystal size is around 2.15 nm. The transfer and output characteristics of corresponding TFTs are shown in Fig. 7(a) and (b). The

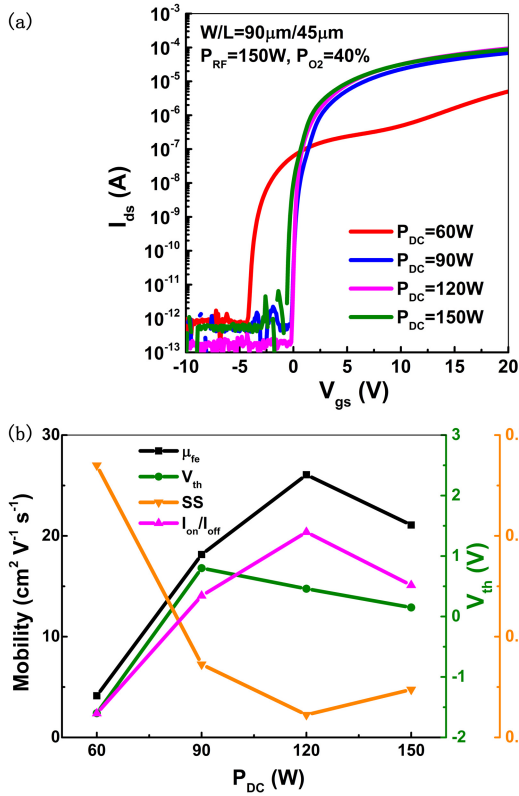


Fig. 6. (a) Transfer curves and (b) key electrical parameter variation of ITO-stabilized ZnO TFTs with hybrid-phase microstructural channels under different P_{DC} .

extracted μ_{fe} , V_{th} , and ON/OFF ratio of a typical device are $26.1 \text{ cm}^2/\text{V}\cdot\text{s}$, 0.5 V , and over 10^9 , respectively. In addition, the value of SS can achieve as low as $89 \text{ mV}/\text{decade}$. It means that the total trap density (N_{total}) in bulk channels and at the gate dielectric/channel interface is maintained at a relatively low level, which is only $2.67 \times 10^{11} \text{ cm}^{-2}\text{eV}^{-1}$. The relationship between N_{total} and SS fulfills the following equation:

$$SS = \frac{q K_B T N_{total}}{C_{ox} \log(e)} \quad (4)$$

where q , k_B , T , and C_{ox} are the electron charge, Boltzmann's constant, absolute temperature, and gate capacitance per unit area, respectively [17], [45]. Fig. 7(c) plots μ_{fe} as a function of gate bias, which is quite similar to the a-IGZO case [1]. At low gate bias, the trap-limited conduction dominates, so the almost abrupt increase of μ_{fe} reflects a low level of carrier trapping, which can be passivated rapidly [46]. At high gate bias, a decrease of μ_{fe} is observed, and this is owing to the increased scattering effects among induced carriers. From output curves, a current crowding effect at low drain voltage is still observed. This indicates the imperfect contacts in source and drain regions. Thus, future optimization work is required to further promote the electrical performance of devices.

Table II lists the key electrical parameters of our hybrid-phase microstructural ITO-stabilized ZnO TFTs as well as some typical ITO, ZnO, and ITZO channel-based TFTs, which were published in recent years. Compared with the general amorphous ITZO TFTs, it is found that μ_{fe} of our devices is fairly competitive. Meanwhile, their SS and ON-OFF ratio

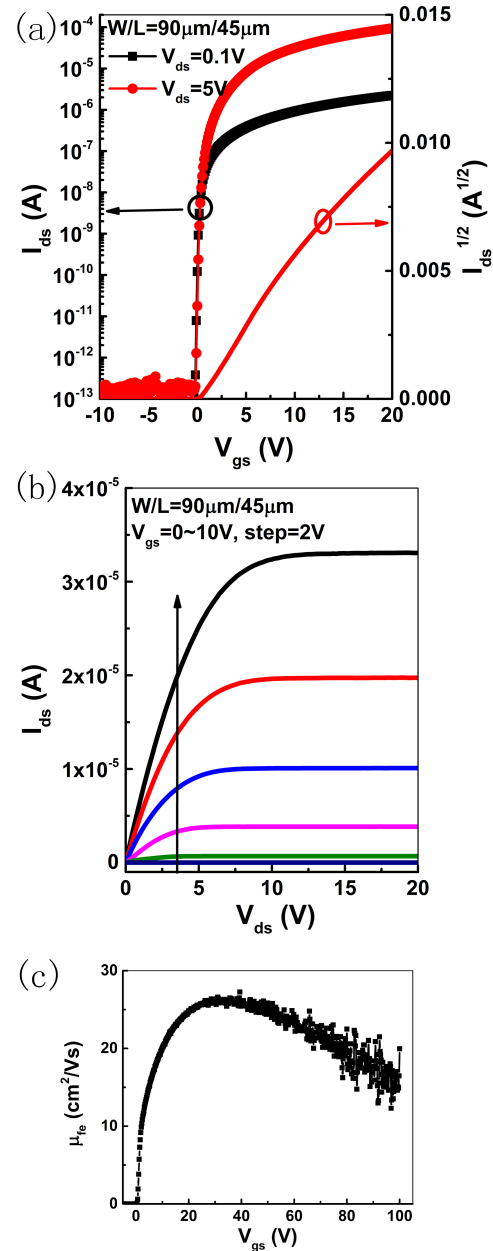


Fig. 7. (a) Transfer curves and (b) output curves of optimal hybrid-phase microstructural ITO-stabilized ZnO TFTs with the basic top-contact bottom-gated architecture. (c) Plot of μ_{fe} as a function of gate bias.

values are among the best ever reported. When it comes to the basic ZnO and ITO TFTs, the electrical performance of devices in this work is also attractive.

The spatially electrical uniformity of TFTs with hybrid-phase microstructural channels is also examined. Fig. 8 describes the key electrical parameters of 30 devices, which are uniformly distributed over a 4-in wafer. Apart from the enhanced device behavior, it is clearly seen that all the key electrical parameters fluctuate within a rather narrow range. Particularly, the relative standard deviations of μ_{fe} and SS are only 3.1% and 8.2%, respectively. It can be concluded that the hybrid-phase microstructure does not deteriorate spatially electrical uniformity of devices. Because the influence of sparse nanocrystals inside the thin films is ignorable,

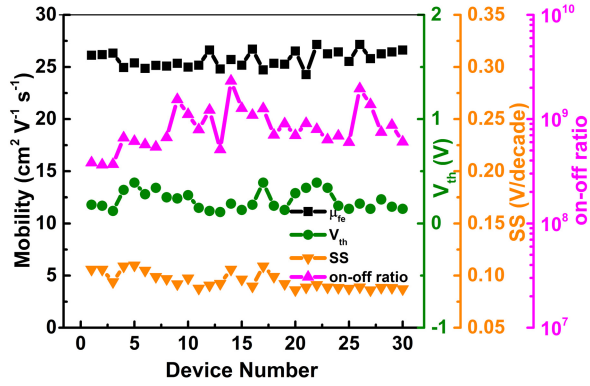


Fig. 8. Spatially electrical parameter uniformity of ITO-stabilized ZnO TFTs with hybrid-phase microstructural channels. Thirty devices that uniformly distributed over a 4-in Si wafer are tested.

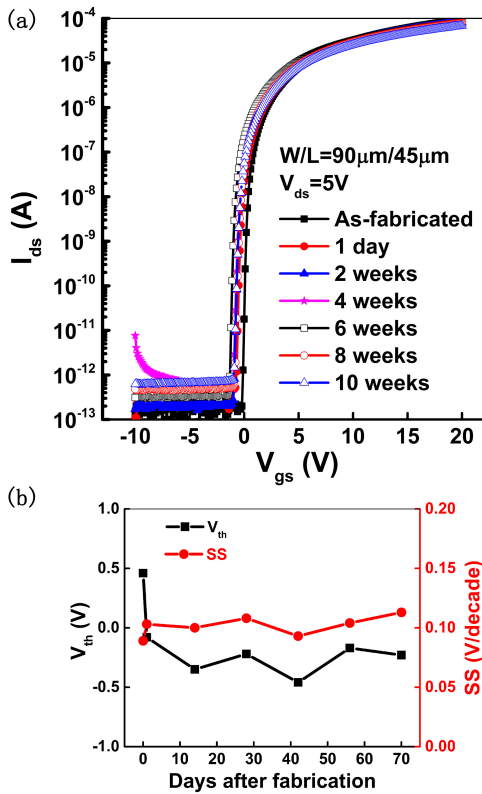


Fig. 9. (a) Transfer curve evolution and (b) V_{th} and SS variation of devices without any passivation, which are placed in air for 10 weeks.

especially when they are analyzed in the dimension of TFT channels. Therefore, such hybrid-phase microstructural TFTs are believed to be compatible with large-area applications.

Furthermore, the ITO-stabilized ZnO TFTs exhibit robustness to the atmospheric ambient, as a result of their unique hybrid-phase microstructural channels. For many ZnO-based devices, there generally exist the ambient interactions at the exposed surface and grain boundaries of ZnO. These oxygen and water adsorption/desorption effects are always accompanied by electron capture/release and trap-state generation, resulting in a severe ambient instability [36], [47], [48]. However, Fig. 9 illustrates that the hybrid-phase microstructural ITO-stabilized ZnO TFTs without any passivation can be operated normally

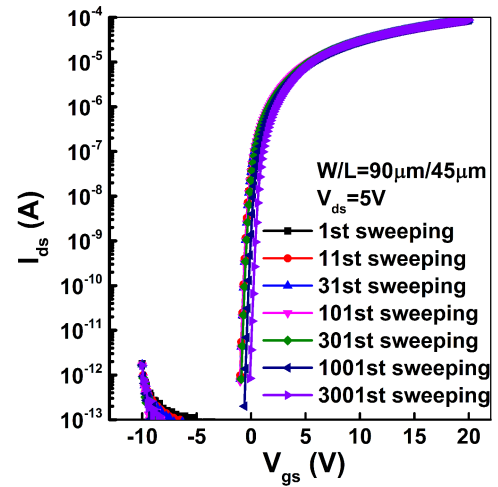


Fig. 10. Transfer curve evolution of the hybrid-phase microstructural ITO-stabilized ZnO TFTs under repeated cycling tests.

only with a small V_{th} fluctuation even after 10 weeks. It is observed that V_{th} of as-fabricated devices drops sharply from about 0.5 V to below zero after half a day, and then its value fluctuates within a narrow range. The ambient interactions seem to achieve a dynamic equilibrium eventually. In addition, there are no stretch-out phenomena observed in subthreshold region of transfer curves, and the extracted values of SS always keep in the vicinity of 0.1 V/decade. It means that few defects are created during this period. Compared with the situations in polycrystalline ZnO and a-IGZO TFTs [49], [50], which are deteriorated significantly after a long term, the TFTs in this work perform extremely atmospheric ambient stable. One plausible explanation is that a large portion of originally exposed ZnO-based backsurface is encapsulated by ITO-involved material, which is less sensitive to the oxygen and water adsorption/desorption processes. Moreover, the grain boundary density in hybrid-phase microstructure is diluted. Therefore, the ambient interactions can be well suppressed, which enables the *in situ* passivation of channels by themselves.

At last, Fig. 10 shows the transfer curve evolution of the hybrid-phase microstructural ITO-stabilized ZnO TFTs under repeated cycling tests. It is found that besides the excellent air stability, such devices also exhibit reliable repeated switching behavior with a slight V_{th} shift of 0.8 V after 3001 sweeping cycles. This is essential in the practical applications.

IV. CONCLUSION

In summary, the properties of hybrid-phase microstructural ITO-stabilized ZnO thin films and the related TFTs were investigated. The optically extracted Urbach energy of thin films revealed less band-tail state trapping compared with that of amorphous thin films, theoretically contributing to higher drift mobility. By adjusting the co-sputtering parameters, the basic top-contact bottom-gated TFTs with optimal active layers could be obtained when P_{O_2} and P_{DC} were set as 40% and 120 W, respectively. The corresponding TFTs exhibited uniform electrical performance with a typical field-effect mobility of 26.1 $\text{cm}^2/\text{V}\cdot\text{s}$, threshold voltage of 0.5 V, ON-OFF ratio of

over 10^9 , and extremely low SS of 89 mV/decade. It was suggested that both material composition and microstructure of active layers should be well taken into the consideration for TFT performance enhancement.

ACKNOWLEDGMENT

The authors would like to thank the Nanosystem Fabrication Facility (NFF-HKUST), Materials Characterization and Preparations Facility (MCPF-HKUST), and the Center for Nanoscale Characterization and Devices (CNCD-WNLO-HUST), for their facility support.

REFERENCES

- [1] E. Fortunato, P. Barquinha, and R. Martins, "Oxide semiconductor thin-film transistors: A review of recent advances," *Adv. Mater.*, vol. 24, no. 22, pp. 2945–2986, Jun. 2012, doi: 10.1002/adma.201103228
- [2] A. Nathan, S. Lee, S. Jeon, and J. Robertson, "Amorphous oxide semiconductor TFTs for displays and imaging," *IEEE/OSA J. Display Technol.*, vol. 10, no. 11, pp. 917–927, Nov. 2014, doi: 10.1109/JDT.2013.2292580.
- [3] J. S. Park, W.-J. Maeng, H.-S. Kim, and J.-S. Park, "Review of recent developments in amorphous oxide semiconductor thin-film transistor devices," *Thin Solid Films*, vol. 520, no. 6, pp. 1679–1693, Jan. 2012, doi: 10.1016/j.tsf.2011.07.018.
- [4] K. Nomura, H. Ohta, A. Takagi, T. Kamiya, M. Hirano, and H. Hosono, "Room-temperature fabrication of transparent flexible thin-film transistors using amorphous oxide semiconductors," *Nature*, vol. 432, no. 4016, pp. 488–492, Nov. 2004, doi: 10.1038/nature03900
- [5] T. Kamiya, K. Nomura, and H. Hosono, "Present status of amorphous In-Ga-Zn-O thin-film transistors," *Sci. Tech. Adv. Mater.*, vol. 11, p. 044305, Sep. 2010, doi: 10.1088/1468-6996/11/4/044305.
- [6] T. M. Pan, B. J. Peng, J. L. Her, and B. S. Lou, "Effect of In and Zn content on structural and electrical properties of InZnSnO thin-film transistors using an Yb_2TiO_5 gate dielectric," *IEEE Trans. Electron Devices*, vol. 64, no. 5, pp. 2233–2238, Mar. 2017, doi: 10.1109/LED.2017.2680410.
- [7] M. H. Cheng, C. Zhao, C. L. Huang, H. Kim, M. Nakata, and J. Kanicki, "Amorphous InSnZnO thin-film transistor voltage-mode active pixel sensor circuits for indirect X-ray imagers," *IEEE Trans. Electron Devices*, vol. 63, no. 12, pp. 4802–4810, Oct. 2016, doi: 10.1109/LED.2016.2615079.
- [8] J. Raja *et al.*, "Improved data retention of InSnZnO nonvolatile memory by H_2O_2 treated Al_2O_3 tunneling layer: A cost-effective method," *IEEE Electron Device Lett.*, vol. 37, no. 10, pp. 1272–1275, Aug. 2016, doi: 10.1109/LED.2016.2599559.
- [9] S. J. Hun, K. K. Suk, M. Y. Gon, C. Rino, and J. J. Kyeong, "Achieving high field-effect mobility exceeding $50 \text{ cm}^2/\text{Vs}$ in In-Zn-Sn-O thin-film transistors," *IEEE Electron Device Lett.*, vol. 35, no. 8, pp. 853–855, Jun. 2014, doi: 10.1109/LED.2014.2329892.
- [10] W. Zhou *et al.*, "Bridged-grain solid-phase-crystallized polycrystalline-silicon thin-film transistors," *IEEE Electron Device Lett.*, vol. 33, no. 10, pp. 1414–1416, Sep. 2012, doi: 10.1109/LED.2012.2210019.
- [11] S. Deng, R. Chen, W. Zhou, J. Y. L. Ho, M. Wong, and H. S. Kwok, "Fabrication of high-performance bridged-grain polycrystalline silicon TFTs by laser interference lithography," *IEEE Trans. Electron Devices*, vol. 63, no. 3, pp. 1085–1090, Mar. 2016, doi: 10.1109/LED.2016.2520081.
- [12] D. Kang *et al.*, "Effect of Ga/In ratio on the optical and electrical properties of GaInZnO thin films grown on SiO_2/Si substrates," *Appl. Phys. Lett.*, vol. 91, p. 091910, Aug. 2007, doi: 10.1063/1.2773952.
- [13] T. Iwasaki *et al.*, "Combinatorial approach to thin-film transistors using multicomponent semiconductor channels: An application to amorphous oxide semiconductors in In–Ga–Zn–O system," *Appl. Phys. Lett.*, vol. 90, p. 242114, Jun. 2007, doi: 10.1063/1.2749177.
- [14] J. Raja, K. Jang, C. P. T. Nguyen, N. Balaji, S. Chatterjee, and J. Yi, "Drain-induced barrier lowering and parasitic resistance induced instabilities in short-channel InSnZnO TFTs," *IEEE Electron Device Lett.*, vol. 35, no. 7, pp. 756–758, Jul. 2014, doi: 10.1109/LED.2014.2318754.
- [15] L. L. Zheng, Q. Ma, Y. H. Wang, W. J. Liu, S. J. Ding, and D. W. Zhang, "High-performance unannealed a-InGaZnO TFT with an atomic-layer-deposited SiO_2 insulator," *IEEE Electron Device Lett.*, vol. 37, no. 6, pp. 743–746, Apr. 2016, doi: 10.1109/LED.2016.2558665.
- [16] P.-T. Liu, Y.-T. Chou, and L.-F. Teng, "Environment-dependent metastability of passivation-free indium zinc oxide thin film transistor after gate bias stress," *Appl. Phys. Lett.*, vol. 95, no. 23, p. 233504, Dec. 2009, doi: 10.1063/1.3272016.
- [17] J. H. Choi *et al.*, "InZnO/AlSnZnInO bilayer oxide thin-film transistors with high mobility and high uniformity," *IEEE Electron Device Lett.*, vol. 37, no. 10, pp. 1295–1298, Aug. 2016, doi: 10.1109/LED.2016.2602284.
- [18] K. Jang, J. Raja, Y.-J. Lee, D. Kim, and J. Yi, "Effects of carrier concentration, indium content, and crystallinity on the electrical properties of indium-tin-zinc-oxide thin-film transistors," *IEEE Electron Device Lett.*, vol. 34, no. 9, pp. 1151–1153, Sep. 2013, doi: 10.1109/LED.2013.2272084.
- [19] S. Yamazaki, Y. Shima, Y. Hosaka, K. Okazaki, and J. Koezuka, "Achievement of a high-mobility FET with a cloud-aligned composite oxide semiconductor," *Jpn. J. Appl. Phys.*, vol. 55, p. 115504, Oct. 2016, doi: 10.7567/JJAP.55.115504.
- [20] A. M. Ma, M. Shen, A. Afshar, Y. Y. Tsui, K. C. Cadien, and D. W. Barlage, "Interfacial contact effects in top gated zinc oxide thin film transistors grown by atomic layer deposition," *IEEE Trans. Electron Devices*, vol. 63, no. 9, pp. 3540–3546, Jul. 2016, doi: 10.1109/LED.2016.2586418.
- [21] Y. H. Wang *et al.*, "Performance improvement of atomic layer-deposited ZnO/ Al_2O_3 thin-film transistors by low-temperature annealing in air," *IEEE Trans. Electron Devices*, vol. 63, no. 5, pp. 1893–1898, Apr. 2016, doi: 10.1109/LED.2016.2540679.
- [22] K. A. Stewart and J. F. Wager, "69-2: Oxide-TFT mobility limits and CMOS feasibility," in *SID Symp. Dig. Tech. Papers*, vol. 47, May 2016, pp. 944–946, doi: 10.1002/sdtp.10881.
- [23] K. A. Stewart, B.-S. Yeh, and J. F. Wager, "Amorphous semiconductor mobility limits," *J. Non-Cryst. Solids*, vol. 432, pp. 196–199, Jan. 2016.
- [24] H. U. Li and T. N. Jackson, "Oxide semiconductor thin film transistors on thin solution-cast flexible substrates," *IEEE Electron Device Lett.*, vol. 36, no. 1, pp. 35–37, Jan. 2015, doi: 10.1109/LED.2014.2371011.
- [25] Y. Shao, X. Xiao, L. Wang, Y. Liu, and S. Zhang, "Anodized ITO thin-film transistors," *Adv. Funct. Mater.*, vol. 24, pp. 4170–4175, Mar. 2014, doi: 10.1002/adfm.201400263.
- [26] Y. Le, Y. Shao, X. Xiao, X. Xu, and S. Zhang, "Indium-tin-oxide thin-film transistors with *in situ* anodized Ta_2O_5 passivation layer," *IEEE Electron Device Lett.*, vol. 37, no. 5, pp. 603–606, Mar. 2016, doi: 10.1109/LED.2016.2548785.
- [27] S. Deng *et al.*, "High-performance staggered top-gate thin-film transistors with hybrid-phase microstructural ITO-stabilized ZnO channels," *Appl. Phys. Lett.*, vol. 109, p. 182105, Oct. 2016, doi: 10.1063/1.4966900.
- [28] S. P. Harvey, K. R. Poepelmeier, and T. O. Mason, "Subsolidus phase relationships in the ZnO– In_2O_3 – SnO_2 system," *J. Amer. Ceram. Soc.*, vol. 91, pp. 3683–3689, Oct. 2008, doi: 10.1111/j.1551-2916.2008.02686.x.
- [29] M. Caglar, S. Ilican, Y. Caglar, and F. Yakuphanoglu, "Electrical conductivity and optical properties of ZnO nanostructured thin film," *Appl. Surf. Sci.*, vol. 255, pp. 4491–4496, Nov. 2008, doi: 10.1016/j.apsusc.2008.11.055.
- [30] K. J. Saji, M. K. Jayaraj, K. Nomura, T. Kamiya, and H. Hosono, "Optical and carrier transport properties of cosputtered Zn-In-Sn-O films and their applications to TFTs," *J. Electrochem. Soc.*, vol. 155, pp. H390–H395, Apr. 2008, doi: 10.1149/1.2903866.
- [31] H. Hosono, "Ionic amorphous oxide semiconductors: Material design, carrier transport, and device application," *J. Non-Cryst. Solids*, vol. 352, nos. 9–20, pp. 851–858, Jun. 2006, doi: 10.1016/j.jnoncrsol.2006.01.073
- [32] Y. Kim *et al.*, "Amorphous InGaZnO thin-film transistors—Part I: Complete extraction of density of states over the full subband-gap energy range," *IEEE Trans. Electron Devices*, vol. 59, no. 10, pp. 2689–2698, Sep. 2012, doi: 10.1109/LED.2012.2208969.
- [33] K. Nomura, A. Takagi, T. Kamiya, H. Ohta, M. Hirano, and H. Hosono, "Amorphous oxide semiconductors for high-performance flexible thin-film transistors," *Jpn. J. Appl. Phys.*, vol. 45, no. 5B, p. 4303, 2006.
- [34] Y. S. Rim, D. L. Kim, W. H. Jeong, and H. J. Kim, "Effect of Zr addition on ZnSnO thin-film transistors using a solution process," *Appl. Phys. Lett.*, vol. 97, p. 233502, Dec. 2010, doi: 10.1063/1.3524514.

- [35] M. G. Yun, C. H. Ahn, S. W. Cho, S. H. Kim, Y. K. Kim, and H. K. Cho, "Dual electrical behavior of multivalent metal cation-based oxide and its application to thin-film transistors with high mobility and excellent photobias stability," *ACS Appl. Mater. Inter.*, vol. 7, pp. 6118–6124, Feb. 2015, doi: 10.1021/am5085836.
- [36] H. Y. Jung *et al.*, "Origin of the improved mobility and photo-bias stability in a double-channel metal oxide transistor," *Sci. Rep.*, vol. 4, p. 3765, Jan. 2014, doi: 10.1038/srep03765.
- [37] M. Yeon-Keon, L. Sih, K. Do-Hyun, L. Dong-Hoon, J. Chang-Oh, and P. Jong-Wan, "Application of DC magnetron sputtering to deposition of InGaZnO films for thin film transistor devices," *Jpn. J. Appl. Phys.*, vol. 48, p. 031301, Mar. 2009, doi: 10.1143/JJAP.48.031301.
- [38] J. Zhang *et al.*, "C-Axis oriented crystalline IGZO thin-film transistors by magnetron sputtering," *J. Mater. Chem. C*, vol. 5, pp. 2388–2396, Jan. 2017, doi: 10.1039/C7TC00193B.
- [39] P. Barquinha, L. Pereira, G. Gonçalves, R. Martins, and E. Fortunato, "Toward high-performance amorphous GIZO TFTs," *J. Electrochem. Soc.*, vol. 156, pp. H161–H168, Sep. 2009, doi: 10.1149/1.3049819.
- [40] R. Hong, H. Qi, J. Huang, H. He, Z. Fan, and J. Shao, "Influence of oxygen partial pressure on the structure and photoluminescence of direct current reactive magnetron sputtering ZnO thin films," *Thin Solid Films*, vol. 473, pp. 58–62, Feb. 2005, doi: 10.1016/j.tsf.2004.06.159.
- [41] R. R. Ghimire and A. K. Raychaudhuri, "High performance thin film transistor (flex-TFT) with textured nanostructure ZnO film channel fabricated by exploiting electric double layer gate insulator," *Appl. Phys. Lett.*, vol. 110, p. 052105, Jan. 2017, doi: 10.1063/1.4975209.
- [42] J.-Y. Noh *et al.*, "Cation composition effects on electronic structures of In-Sn-Zn-O amorphous semiconductors," *J. Appl. Phys.*, vol. 113, p. 183706, May 2013, doi: 10.1063/1.4803706.
- [43] B. Kumar, H. Gong, and R. Akkipeddi, "A study of conduction in the transition zone between homologous and ZnO-rich regions in the In₂O₃-ZnO system," *J. Appl. Phys.*, vol. 97, p. 063706, Mar. 2005, doi: 10.1063/1.1862311.
- [44] S. H. Kim, C. H. Ahn, M. G. Yun, S. W. Cho, and H. K. Cho, "Anomalous tin chemical bonding in indium-zinc-tin oxide films and their thin film transistor performance," *J. Phys. D, Appl. Phys.*, vol. 47, p. 485101, Nov. 2014, doi: 10.1088/0022-3727/47/48/485101.
- [45] S. M. Sze and K. K. Ng, *Physics of Semiconductor Devices*. Hoboken, NJ, USA: Wiley, 2006.
- [46] S. Lee *et al.*, "Trap-limited and percolation conduction mechanisms in amorphous oxide semiconductor thin film transistors," *Appl. Phys. Lett.*, vol. 98, no. 20, p. 203508, May 2011, doi: 10.1063/1.3589371.
- [47] J. K. Jeong, H. W. Yang, J. H. Jeong, Y.-G. Mo, and H. D. Kim, "Origin of threshold voltage instability in indium-gallium-zinc oxide thin film transistors," *Appl. Phys. Lett.*, vol. 93, no. 12, p. 123508, Sep. 2008, doi: 10.1063/1.2990657.
- [48] R. B. M. Cross and M. M. De Souza, "Investigating the stability of zinc oxide thin film transistors," *Appl. Phys. Lett.*, vol. 89, no. 26, p. 263513, Dec. 2006, doi: 10.1063/1.2425020.
- [49] K.-T. Kim, K. Lee, M. S. Oh, C. H. Park, and S. Im, "Surface-induced time-dependent instability of ZnO based thin-film transistors," *Thin Solid Films*, vol. 517, pp. 6345–6348, Oct. 2009, doi: 10.1016/j.tsf.2009.02.093.
- [50] P.-T. Liu, Y.-T. Chou, L.-F. Teng, F.-H. Li, C.-S. Fuh, and H.-P. D. Shieh, "Ambient stability enhancement of thin-film transistor with InGaZnO capped with InGaZnO:N bilayer stack channel layers," *IEEE Electron Device Lett.*, vol. 32, no. 10, pp. 1397–1399, Oct. 2011, doi: 10.1109/LED.2011.2163181.



Rongsheng Chen (M'16) received the Ph.D. degree from the Department of Electronic and Computer Engineering, The Hong Kong University of Science and Technology, Hong Kong, in 2013.

His current research interests include novel compound thin-film transistors based on ZnO, IGZO, GaN, and their application in active matrix displays.



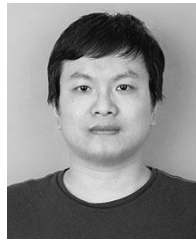
Guijun Li received the Ph.D. degree from the Department of Electronic and Computer Engineering, The Hong Kong University of Science and Technology, Hong Kong, in 2013.

His current research interests include perovskite and silicon-based photovoltaic devices.



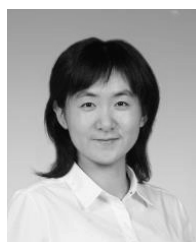
Zhihe Xia is currently pursuing the Ph.D. degree with the Department of Electronic and Computer Engineering, The Hong Kong University of Science and Technology, Hong Kong.

His current research interests include IGZO TFTs and ITZO TFTs with advanced device architecture.



Meng Zhang (M'17) received the Ph.D. degree from the Department of Electronic and Computer Engineering, The Hong Kong University of Science and Technology, Hong Kong, in 2016.

His current research interests include novel thin-film transistor (TFT) structures, oxide TFTs, and reliability of TFTs.



Wei Zhou received the Ph.D. degree from the Department of Electronic and Computer Engineering, The Hong Kong University of Science and Technology, Hong Kong, in 2013.

Her current research interests include low-temperature poly-Si thin-film transistors (TFTs), novel-oxide TFTs, and their application in displays.



Man Wong (M'84-SM'00) received the Ph.D. degree in electrical engineering from the Center for Integrated Systems, Stanford University, Palo Alto, CA, USA.

In 1992, he joined the Department of Electrical and Electronic Engineering, The Hong Kong University of Science and Technology, Hong Kong, as a Faculty Member.



Hoi-Sing Kwok (M'78-SM'84-F'05) received the Ph.D. degree in applied physics from Harvard University, Cambridge, MA, USA, in 1978.

He joined The Hong Kong University of Science and Technology, Hong Kong, in 1992, where he is currently the Director of the Center for Display Research and the State Key Laboratory on Advanced Displays and Optoelectronics Technologies.



Sunbin Deng received the B.S. degree in optical information science and technology from the Huazhong University of Science and Technology, Wuhan, China, in 2014. He is currently pursuing the Ph.D. degree with the Department of Electronic and Computer Engineering, The Hong Kong University of Science and Technology, Hong Kong.

His current research interests include poly-Si, metal-oxide, and novel material thin-film transistors.